Water wave scattering by finite arrays of circular structures

P. G. CHAMBERLAIN†

Department of Mathematics, The University of Reading, PO Box 220,
Whiteknights, Reading RG6 6AX, UK

The scattering of small amplitude water waves by a finite array of locally axisymmetric structures is considered. Regions of varying quiescent depth are included and their axisymmetric nature, together with a mild-slope approximation, permits an adaptation of well-known interaction theory which ultimately reduces the problem to a simple numerical calculation. Numerical results are given and effects due to regions of varying depth on wave loading and free-surface elevation are presented.

Keywords: surface wave scattering; topography; interaction theory.

1. Introduction

The scattering of water waves by natural or man-made structures is a long-standing problem of widespread interest. Explicit expressions for analytic solutions to the modelling equations are rare and problems involving 'realistic' domains will typically require some computational effort, if those solutions are to be approximated.

Often, if the domain of the problem is of a special type, then some analytic progress can be made to facilitate any numerical procedure. For example, if the depth contours are concentric circles, then solutions may be sought in terms of the independent radial variable (see, e.g. Chamberlain & Porter, 1999). Recently, Hughes (2005) was able to make progress in this area on the assumption that depth contours were confocal ellipses.

In this paper, we will consider the scattering of water waves by a finite array of locally axisymmetric structures. This problem area includes the possibility of an array of submerged islands, or of surface-piercing cylinders or of a combination of the two types of structures.

Motivated in part by the significant engineering applications, much of the relevant existing literature has concentrated on arrays of identical vertical cylinders. One contribution is that by Linton & Evans (1990) who adapted the interaction theory of Spring & Monkmeyer (1974) to derive simple formulae for wave forcing and free-surface amplitude. The interaction theory has been used by many authors (see Walker & Eatock Taylor, 2005, for a recent survey of the work that has been carried out) and we will adapt it for our purposes in what follows here.

Our approach will be to adapt the interaction theory to allow for regions of varying quiescent depth. Thus, we may think of a submerged circular island or of a bottom-mounted cylinder with a footing structure at its base or of a circular island with an underwater shoal (such as that considered by Homma, 1950, e.g.). The case of a single circular structure was dealt with using a mild-slope approximation by Chamberlain & Porter (1999), and this paper extends some of the results of that publication to problems involving more than one structure. Chamberlain (2004) has given evidence that the

---

†Email: p.g.chamberlain@reading.ac.uk

evanescent modes have little qualitative effect in the related problem of wave scattering by a single axisymmetric structure and we will model the scattered wave in this paper using only the travelling waves.

The 'classical' mild-slope equation was derived independently by Berkhoff (1973, 1976) and Smith & Sprinks (1975), and its range of validity was later extended in the modified mild-slope equation of Chamberlain & Porter (1995). The most important part of Chamberlain & Porter's improvement was in retaining a term involving second derivatives of the quiescent depth h. The appearance of $\nabla^2 h$, where ∇ is the gradient operator, in the modified mild-slope equation implies (Porter & Staziker, 1995) that matching conditions must be applied to the dependent variable when ∇h is discontinuous, but we will avoid this technicality using a variable change proposed by Porter (2003).

Silva *et al.* (2005) developed a numerical method for the modified mild-slope equation (their model also includes energy dissipation) and presented a selection of results for problems involving arrays of cylinders between which the quiescent depth is allowed to vary. Their approach could be used for the problems considered in this paper, but the aim here is to restrict attention to depth profiles that vary in a way that facilitates the development of a method requiring only very simple numerical calculations. The (locally) axisymmetric nature of the scatterers implies that the numerical effort can be reduced to the solution of some initial-value problems and then of a linear system of equations.

The plan of the paper is as follows. In Section 2, we review the mild-slope approximations that we will use and in Section 3, the interaction theory is adapted to our present purposes. In Sections 4 and 5, we give expressions for the far field coefficient and wave-loading forces. Numerical results are given in Section 6 and conclusions are summarized in Section 7.

2. Mild-slope approximations

Let (x, y, z) be the Cartesian coordinates arranged so that $z = 0$ corresponds to the quiescent free-surface position of an incompressible fluid in an irrotational motion. Polar coordinates defined by $x = r \cos \theta$ and $y = r \sin \theta$ will also be used. Usual assumptions imply the existence of a complex-valued velocity potential $\Psi(x, y, z, t) = \psi(x, y, z)e^{-i\omega t}$, assuming periodic time dependence. The (complex-valued) free-surface elevation, with time dependence removed, is given by

$$\eta(x, y) = \frac{i\omega}{g} \psi(x, y, 0),$$

where g is the acceleration due to gravity.

Anticipating the use of a mild-slope approximation, ψ for $z \in (-h, 0)$, where $h = h(x, y)$ is the quiescent depth, may be estimated from η as

$$\psi(x, y, z) \approx \frac{g}{i\omega} \eta(x, y) \frac{\cosh \kappa(z + h)}{\cosh \kappa h},$$

in which $\kappa = \kappa(h) > 0$ satisfies the local dispersion relation

$$\kappa \tanh(\kappa h) = K \equiv \omega^2/g.$$

The modified mild-slope equation (Chamberlain & Porter, 1995) may be written as

$$\nabla \cdot u \nabla \eta + v \eta = 0, \tag{2.1}$$

where $u = u(h) = (2\kappa h + \sinh(2\kappa h))/4\kappa \cosh^2(\kappa h) > 0$ and $v = v(h) = \kappa^2 u + u_1(\nabla h)^2 + u_2 \nabla^2 h$. The functions $u_1 = u_1(h)$ and $u_2 = u_2(h)$ will not be referred to again after this section and their definitions,

which are given in Chamberlain & Porter (1995), are omitted. Following the recent reappraisal of the mild-slope approximation by Porter (2003), we change the dependent variable in (2.1) by defining

$$\phi = \eta \kappa(h)\sqrt{u(h)}/\kappa_0\sqrt{u(h_0)}, \tag{2.2}$$

a constant denominator has been included in (2.2) so that ϕ and η coincide when $h = h_0$, the depth at large r. Here, $\kappa_0 = \kappa(h_0)$. This change of variable leads to

$$\nabla \cdot \kappa^{-2}\nabla\phi + (1 - w(\nabla h)^2)\phi = 0, \tag{2.3}$$

in which

$$w(h) = \frac{3(2\tilde{\kappa} + \sinh\tilde{\kappa})(\sinh 2\tilde{\kappa} - \sinh\tilde{\kappa}) - 3\tilde{\kappa}^2(\cosh 2\tilde{\kappa} + 2) - 4\tilde{\kappa}^3\sinh\tilde{\kappa} - \tilde{\kappa}^4}{3(\tilde{\kappa} + \sinh\tilde{\kappa})^2},$$

where $\tilde{\kappa} = 2\kappa h$.

Equations (2.3) and (2.1) are equivalent, since they differ only by a change of variable, but (2.3) has a number of advantages over (2.1). Firstly, there is no need to know (or approximate) second derivatives of h, and the absence of $\nabla^2 h$ implies that $\nabla\phi$ is continuous even when ∇h is not. This fact simplifies the analysis and the calculation of numerical solutions to (2.3) when compared with (2.1) since $\nabla\eta$ will, in general, be discontinuous when ∇h is discontinuous, as shown by Porter & Staziker (1995).

Another advantage that (2.3) has over (2.1) manifests itself when simplifying the equation. If u_1 and u_2 are neglected in the definition of v in (2.1) then the classical mild-slope equation emerges (Berkhoff, 1973, 1976, or Smith & Sprinks, 1975), and a great deal of work has been done in the last 30 years in attempts to patch that approximation (see, e.g. Kirby, 1986) in cases where the results are disappointing, i.e. in cases where ∇h is discontinuous or rapidly varying. The problem with the final step taken to derive the mild-slope equation is the neglect of u_2; it is not always justified to disregard the term involving $\nabla^2 h$. No such problem arises when carrying out the analogous step to simplify (2.3), for there is no appearance of $\nabla^2 h$, and neglect of $w(\nabla h)^2$ leads to a revised mild-slope equation

$$\nabla \cdot \kappa^{-2}\nabla\phi + \phi = 0, \tag{2.4}$$

which (as shown by Porter, 2003) avoids the deficiencies of the classical mild-slope equation, in that effects due to $\nabla^2 h$ have not been removed.

For the time being, in the interests of generality, we will retain the term $w(h)(\nabla h)^2$ in (2.3). There will be some discussion in Section 6 concerning how results are changed when (2.4) is used instead of (2.3).

3. A scattering problem

In this section, we define the scattering problem and adapt the well-known interaction theory (see, e.g. Linton & Evans, 1990) for our present purposes.

We suppose that an incident wave train is scattered by an array of N circular features centred at (x_j, y_j), for $j = 1, 2, \ldots, N$. Polar coordinates (r_j, θ_j) local to these features such that $x - x_j = r_j\cos\theta_j$ and $y - y_j = r_j\sin\theta_j$ will be used in what follows. The jth scatterer has radius $b_j > 0$ and these radii are constrained so that no two scatterers overlap, i.e. $R_{jk} \equiv ((x_j - x_k)^2 + (y_j - y_k)^2)^{1/2} \geqslant b_j + b_k$ for $j, k = 1, 2, \ldots, N$, where $j \neq k$. It is convenient at this stage to define $\mathcal{D} = \mathbb{R}^2 \setminus \cup_{k=1}^N \{(x, y): (x - x_k)^2 + (y - y_k)^2 \leqslant b_k^2\}$, which is a part of the (x, y) plane excluding the circular regions $r_k \leqslant b_k, k = 1, 2, \ldots, N$.

Angles α_{jk} are defined by

$$x_k - x_j = R_{jk} \cos \alpha_{jk}, \quad y_k - y_j = R_{jk} \sin \alpha_{jk},$$

so that the relative positions of scattering structure centres can be inferred from R_{jk} and α_{jk}. Figure 1 summarizes some of the notations that we will use.

The quiescent depth h is taken to be equal to h_0 for all points (x, y) that are not within one of the disjoint circular regions defined above, i.e. when $r_j > b_j$ for all $j = 1, 2, \ldots, N$. We will say more, in Section 3.1, about what form the scattering structures take for $r_j < b_j$ ($j = 1, 2, \ldots, N$).

We suppose that waves are incident at an angle β to the x-axis and take an incident wave given by

$$\phi_I = e^{i\kappa_0 r \cos(\theta - \beta)} = I_j(\beta) e^{i\kappa_0 r_j \cos(\theta_j - \beta)},$$

in which $I_j(\beta) = e^{i\kappa_0(x_j \cos \beta + y_j \sin \beta)}$ is a phase term that allows us to write ϕ_I in terms of any of the scatterer-centred polar coordinates defined above. This incident wave may be written as

$$\phi_I = I_j(\beta) \sum_{m=-\infty}^{\infty} J_m(\kappa_0 r_j) e^{im(\frac{\pi}{2} + \theta_j - \beta)}. \tag{3.1}$$

We require the scattered wave to be outgoing at infinity; to be consistent with the mild-slope approximation, we omit evanescent waves and write

$$\phi_S(x, y) = \sum_{m=-\infty}^{\infty} \sum_{j=1}^{N} B_m^j H_m(\kappa_0 r_j) e^{im\theta_j}, \quad (x, y) \in \mathcal{D}, \tag{3.2}$$

where H_m is a Hankel function of the first kind. The coefficients B_m^j must be found as part of the solution procedure. This expression for ϕ_S omits the term Z_m denoted by Linton & Evans (1990); the difference is only a notational one and reflects the fact that the significant algebraic advantage offered by Z_m only arises when the scatterer is a vertical cylinder and our aim here is to consider more general structures.
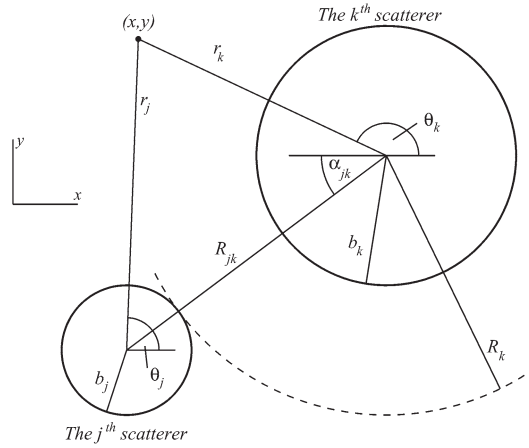

FIG. 1. Plan view sketch showing notation relevant to the jth and the kth scatterers. It is assumed here that the jth scatterer is the one closest to the kth; this fact allows us to show R_k on the diagram.

We now fix the integer k (where $1 \leqslant k \leqslant N$) and consider the effect of and on the scatterer centred at (x_k, y_k). We use Graf's addition theorem for Bessel functions (Gradshteyn & Ryzhik, 1965, p. 979, equation WA394(6)) to write the expression for ϕ_S in terms of the polar coordinates (r_k, θ_k) that leads to

$$\phi_S(x, y) = \sum_{m=-\infty}^{\infty} \left[B_m^k H_m(\kappa_0 r_k) \mathrm{e}^{\mathrm{i}m\theta_k} + \sum_{j=1, j\neq k}^{N} B_m^j \sum_{p=-\infty}^{\infty} J_p(\kappa_0 r_k) H_{m-p}(\kappa_0 R_{jk}) \mathrm{e}^{\mathrm{i}p\theta_k} \mathrm{e}^{\mathrm{i}(m-p)\alpha_{jk}} \right],$$

(3.3)

which is valid at points $(x, y) \in \mathcal{D}$ which also satisfy $r_k < R_k \equiv \min_{j=1, j\neq k}^{N}(R_{jk} - b_j)$. The quantity R_k is the largest radius around the kth scatterer which does not intersect any part of another scatterer. It is worth noting that the addition theorem for Bessel functions is valid for a larger range of r_k than that mentioned here, but the definition of R_k is sufficient in what follows and it is convenient later to be able to note that the quiescent depth h is equal to h_0 for all $r_k \in [b_k, R_k]$.

It simplifies matters that are to follow if we define $\phi_m^k(r_k)$ as the coefficient of $\mathrm{e}^{\mathrm{i}m\theta_k}$ near (x_k, y_k), i.e.

$$\phi = \phi_I + \phi_S = \sum_{m=-\infty}^{\infty} \phi_m^k(r_k) \mathrm{e}^{\mathrm{i}m\theta_k} \quad (r_k < R_k).$$

Equations (3.1) and (3.2) can now be used to deduce that

$$\phi_m^k(r_k) = \lambda_m^k J_m(\kappa_0 r_k) + B_m^k H_m(\kappa_0 r_k) \quad (b_k \leqslant r_k \leqslant R_k),$$

(3.4)

where

$$\lambda_m^k = I_k(\beta) \mathrm{e}^{\mathrm{i}m(\frac{\pi}{2}-\beta)} + \sum_{j=1 \ j\neq k}^{N} \sum_{p=-\infty}^{\infty} B_p^j H_{p-m}(\kappa_0 R_{jk}) \mathrm{e}^{\mathrm{i}(p-m)\alpha_{jk}}.$$

The term λ_m^k is a measure of all the waves incident on the kth scatterer in the mth angular mode. The first term in λ_m^k is part of ϕ_I and the summation gathers together waves diffracted from scatterers other than the kth.

We have now reached a point where it is useful to be a little more specific about the scattering structure in $r_k < b_k$.

3.1 Wave-scattering structures

We list the three types of wave-scattering structure to be considered in this paper. In each case, we suppose that the scatterer centred at (x_k, y_k) can be defined independently of θ_k, i.e. each scatterer is locally axisymmetric.

Suppose that we now restrict attention to points (x, y) such that $(x - x_k)^2 + (y - y_k)^2 < R_k^2$, it now follows that (2.3) reduces to

$$(\kappa^{-2} r_k \phi_m^{k\prime})' + (r_k(1 - wh'^2) - r_k^{-1} m^2 \kappa^{-2}) \phi_m^k = 0 \quad (a_k < r_k, \ 0 \leqslant \theta_k < 2\pi),$$

since $h = h(r_k)$ where $'$ denotes differentiation with respect to the radial derivative r_k and it will prove convenient later to have defined the first-order system

$$\begin{pmatrix} R_m^k \\ \kappa^{-2} r_k R_m^{k\prime} \end{pmatrix}' = \begin{pmatrix} 0 & \kappa^2 r_k^{-1} \\ r_k^{-1} m^2 \kappa^{-2} - r_k(1 - wh'^2) & 0 \end{pmatrix} \begin{pmatrix} R_m^k \\ \kappa^{-2} r_k R_m^{k\prime} \end{pmatrix}.$$
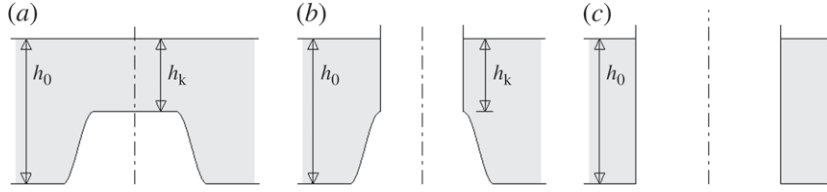
(3.5)

FIG. 2. Radial cross-section sketches of the three types of wave-scattering structure considered in this paper. Subplot (a) is an example of a submerged island, (b) is a surface-piercing structure with a shoal and (c) is a bottom-mounted cylinder. In each case, the centre line corresponds to $r_k = 0$.

Clearly, ϕ_m^k can be found as a constant multiple of R_m^k, and we will exploit this fact in the three cases below.

3.1.1 *A submerged island.* In this case, the depth profile h is supposed to be continuous and equal to a constant h_k within the circle $r_k < a_k$, for some $a_k < b_k$ (see Fig. 2a). That is

$$h = \begin{cases} h_k, & r_k \leqslant a_k, \\ h_0, & b_k \leqslant r_k \leqslant R_k. \end{cases}$$

The radial derivative h' is assumed to be continuous everywhere except, possibly, at $r_k = a_k$ and $r_k = b_k$.

We now specify which solutions to (3.5) are appropriate in the present case. In the region $r_k < a_k$, we reject unbounded Bessel functions on the grounds that they are unphysical and take

$$\phi_m^k = A_m^k J_m(\kappa_k r_k) \quad (r_k \leqslant a_k),$$

where $\kappa_k = \kappa(h_k)$. The coefficients A_m^k will be found as part of the solution procedure.

It is now clear that if, in addition to (3.5), we impose

$$R_m^k(a_k) = J_m(\kappa_k a_k), \quad R_m^{k\,\prime}(a_k) = \kappa_k J_m'(\kappa_k a_k), \tag{3.6}$$

then it follows that $\phi_m^k(r_k) = A_m^k R_m^k(r_k)$ for $a_k \leqslant r_k \leqslant b_k$.

One advantage in defining R_m^k and then seeking ϕ_m^k subsequently is that the initial-value problem (3.5) and (3.6) is entirely real valued. The complex-valued nature of ϕ_m^k is wholly due to the coefficient A_m^k.

Note that in deriving (3.6), we have used the fact that $\phi_m^{k\,\prime}$ is continuous at $r_k = a_k$, even though h' is allowed to be discontinuous there. This helpful fact is a feature of using (2.3) and solving for ϕ and would not be the case if we were using (2.1) and solving for η.

The values $R_m^k(b_k)$ and $R_m^{k\,\prime}(b_k)$, which emerge from a solution to the initial-value problem (3.5) and (3.6), will be referred to later when expressions for the solution in $r_k > b_k$ are derived.

3.1.2 *A surface-piercing structure surrounded by a shoal.* Here, we suppose that h varies in $a_k < r_k < b_k$ and that a circular cylinder of radius a_k centred at (x_k, y_k) surmounts the bedform, see Fig. 2(b). This situation may be thought of as a model for an axisymmetric island, see e.g. Homma (1950), or for a bottom-mounted circular cylinder with an axisymmetric footing structure at its base. Here, as in Section 3.1.1, we seek a solution of (3.5) and appropriate initial conditions to use in conjunction with that system are

$$R_m^k(a_k) = 1, \quad R_m^{k\,\prime}(a_k) = 0,$$

so that $\phi_m^k(r_k) = A_m^k R_m^k(r_k)$ for $a_k \leqslant r_k \leqslant b_k$, for some A_m^k that are to be found.

The values $R_m^k(b_k)$ and $R_m^{k\,\prime}(b_k)$ are found by solving the initial-value problem and will be referred to later.

3.1.3 *A bottom-mounted cylinder.*

In this case, we suppose that the scatterer takes the form of a vertical cylinder of radius b_k, which meets the flat bottom at $z = -h_0$, see Fig. 2(c). This form of scatterer involves no (local) region of varying quiescent depth and has been considered by many authors, we include it here for completeness. Here, we simply require that

$$\phi_m^{k\,\prime}(b_k) = 0.$$

In order that this case can be dealt with using a notation containing the two cases in Sections 3.1.1 and 3.1.2, we define $R_m^k(b_k) = 1$, $R_m^{k\,\prime}(b_k) = 0$ and let

$$\phi_m^k(b_k) = A_m^k R_m^k(b_k) = A_m^k,$$

this last equation defines the quantity A_m^k for scatterers of this type.

It is notationally convenient if we set $a_k = b_k$, in particular, therefore it follows that $R_m^k(a_k) = 1$.

3.2 *Implementation*

In each of the three cases discussed above, we found that

$$\phi_m^k(b_k) = A_m^k R_m^k(b_k), \quad \phi_m^{k\,\prime}(b_k) = A_m^k R_m^{k\,\prime}(b_k), \tag{3.7}$$

where $R_m^k(b_k)$ and $R_m^{k\,\prime}(b_k)$ are either found via an initial-value problem (as in Sections 3.1.1 and 3.1.2) or known by definition (as in Section 3.1.3). Eliminating the unknown coefficient A_m^k, we obtain

$$\phi_m^{k\,\prime}(b_k) R_m^k(b_k) - \phi_m^k(b_k) R_m^{k\,\prime}(b_k) = 0. \tag{3.8}$$

The next step is to combine (3.8), which was derived from inside the circle $r_k = b_k$, with (3.4) which is valid for $b_k < r_k < R_k$. This matching is easily carried out since we know that $\phi_m^{k\,\prime}$ is continuous even if ∇h is discontinuous at $r_k = b_k$, and we find that

$$\lambda_m^k \mathrm{Re}(Y_m^k) + B_m^k Y_m^k = 0, \quad k = 1, 2, \ldots, N, \quad m \in \mathbb{Z},$$

which is an infinite system of equations for the scattering coefficients B_m^k. Here, $Y_m^k \equiv \kappa_0 R_m^k(b_k) H_m'(\kappa_0 b_k) - R_m^{k\,\prime}(b_k) H_m(\kappa_0 b_k)$ is never zero, since if it vanishes then the consideration of its real and imaginary parts would imply that $R_m^k(b_k) = R_m^{k\,\prime}(b_k) = 0$, and the functions R_m^k and $R_m^{k\,\prime}$ cannot be zero simultaneously. We conclude that $Y_m^k \neq 0$ for $k = 1, 2, \ldots, N$ and $m \in \mathbb{Z}$.

We can find the coefficients A_m^k by using (3.7) to form an expression for $A_m^k Y_m^k$, leading to

$$A_m^k = \frac{2\mathrm{i}\lambda_m^k}{\pi b_k Y_m^k}, \tag{3.9}$$

by using a Wronskian to simplify the right-hand side.

When seeking numerical solutions, we must replace infinite sums with finite ones. We choose a natural number M and write

$$\phi_S \approx \tilde{\phi}_S = \sum_{m=-M}^{M} \sum_{j=1}^{N} \tilde{B}_m^j H_m(\kappa_0 r_j) \mathrm{e}^{\mathrm{i} m \theta_j},$$

in which approximations $\tilde{B}_m^k$ to a finite number of the coefficients B_m^k are found from the system of $(2M + 1)N$ equations

$$\tilde{\lambda}_m^k \text{Re}(Y_m^k) + \tilde{B}_m^k Y_m^k = 0, \quad k = 1, 2, \ldots, N, \quad m = -M, \ldots, M, \tag{3.10}$$

where Y_m^k is as given earlier and

$$\tilde{\lambda}_m^k = I_k(\beta)e^{im(\frac{\pi}{2} - \beta)} + \sum_{j=1 j \neq k}^{N} \sum_{p=-M}^{M} \tilde{B}_p^j H_{p-m}(\kappa_0 R_{jk})e^{i(p-m)\alpha_{jk}}.$$

Once (3.10) has been solved for $\tilde{B}_m^k$, we can evaluate $\tilde{\lambda}_m^k$ and hence find

$$A_m^k \approx \tilde{A}_m^k = \frac{2i\tilde{\lambda}_m^k}{\pi b_k Y_m^k},$$

which can be used to approximate ϕ in $r_k < b_k$.

4. Far-field solution

Here, we find an expression for the scattered wave for large values of r. Another application of Graf's addition theorem leads to

$$H_m(\kappa_0 r_k)e^{im\theta_k} = \sum_{n=-\infty}^{\infty} J_n(\kappa_0 \rho_k) H_{m+n}(\kappa_0 r)e^{i(m+n)\theta} e^{-in\psi_k},$$

in which $r = \rho_k$ and $\theta = \psi_k$ are the polar coordinates of (x_k, y_k). Substituting this expression into (3.2), anticipating the truncation of infinite sums for numerical purposes and replacing each appearance of H_{m+p} with its large argument asymptotic approximation, we obtain

$$\phi_S \approx \tilde{\phi}_S = \sum_{m=-M}^{M} \sum_{k=1}^{N} B_m^k H_m(\kappa_0 r_k)e^{im\theta_k} \approx \frac{e^{i\kappa_0 r}}{\sqrt{r}} \sum_{m=-M}^{M} \sum_{k=1}^{N} B_m^k \mathcal{F}_m^k(\theta) = \frac{e^{i\kappa_0 r}}{\sqrt{r}}\mathcal{F}(\beta, \theta) \text{ (say)}, \tag{4.1}$$

for large r, where

$$\mathcal{F}_m^k(\theta) = \sqrt{\frac{2}{\kappa_0 \pi}} \sum_{n=-M}^{M} J_n(\kappa_0 \rho_k)e^{i((m+n)(\theta - \frac{\pi}{2}) - n\psi_k - \frac{\pi}{4})}.$$

5. Forces

The forces acting on the cylindrical parts of the scattering structures may be found by integrating the pressure over the cylinder's surface. We suppose that the jth scatterer is of the type shown in Fig. 2(b) or 2(c) and then the force acting on the cylindrical part of the structure is the real part of

$$(X^j, Y^j)e^{-i\omega t} = \rho \int_{-h_j}^{0} \int_{0}^{2\pi} \frac{\partial \Psi}{\partial t}(\cos\theta_j, \sin\theta_j)a_j \, d\theta_j \, dz$$

$$\approx -e^{-i\omega t} \rho g a_j \int_{-h_j}^{0} \frac{\cosh\kappa_j(z + h_j)}{\cosh\kappa_j h_j} dz \int_{0}^{2\pi} [\eta]_{r_j = a_j}(\cos\theta_j, \sin\theta_j)d\theta_j$$

$$= e^{-i\omega t} \frac{\rho g a_j}{\kappa_j} \tanh\kappa_j h_j \frac{\kappa_0 \sqrt{u(h_0)}}{\kappa_j \sqrt{u(h_j)}}(i(A_{-1}^j + A_1^j), A_{-1}^j - A_1^j),$$

in which ρ is density, since $R_m^j(a_j) = 1$ for scatterers of the type under consideration in this section. The appearances of $\kappa\sqrt{u}$ are a consequence of (2.2).

6. Numerical results

In this section, we consider two test problems. The first is a new example involving a small array of submerged islands and the second is based on a test problem considered by Maniar & Newman (1997). The second test problem involves an array of vertical cylinders and typifies those that have received a great deal of attention (as briefly discussed in Section 1). Here, we will investigate how certain amplifications in wave force and free-surface elevation might be reduced by the introduction of a shoal or footing structure.

Numerical calculations have been carried out using MATLAB. Examples involving scattering structures of the types seen in Fig. 2(a) or 2(b) involve a region of varying quiescent depth and therefore require us to approximate a solution of the System (3.5). Approximations were found using an error-checking Runge–Kutta method.

The choice $M = 6$ was made for computations. This value is consistent with what other authors have used in the constant depth case and an extensive experimentation has shown that larger values of M do not significantly alter any of what follows.

Earlier, we presented two models ((2.3) and (2.4)) for approximating wave motion above regions of varying depth. In what follows, the results presented are mainly for the full model (2.3), but we show the effect of the mild-slope reduction (2.4) for each test problem.

6.1   *Test problem involving submerged topography*

Here, we consider a particular arrangement of four submerged islands. Much of the geometry of the problem is summarized in Table 1.

We choose the topography of each island as follows:

$$h = \begin{cases} h_0 + (h_1 - h_0)((r_1 - b_1)/(a_1 - b_1))^2, & a_1 < r_1 < b_1, \\[2mm] \frac{1}{2}(h_0 + h_2) - \frac{1}{2}(h_2 - h_0)\cos((r_2 - b_2)/(a_2 - b_2)), & a_2 < r_2 < b_2, \\[2mm] h_0 + (h_3/h_0)((r_3 - b_3)/(a_3 - b_3)), & a_3 < r_3 < b_3, \\[2mm] \frac{1}{2}(h_0 + h_4) - \frac{1}{2}(h_4 - h_0)\cos((r_4 - b_4)/(a_4 - b_4)), & a_4 < r_4 < b_4, \end{cases}$$

these representing a conical shoal ($j = 3$), a quadratic shoal with a discontinuity in ∇h at $r_1 = a_1$ and two cosine-shaped shoals ($j = 2$ and $j = 4$).

TABLE 1 *Island centres, radii and central quiescent depth definitions for the submerged topography test problem*

j	x_j/h_0	y_j/h_0	a_j/h_0	b_j/h_0	h_j/h_0
1	5.0	8.0	2.0	4.0	0.50
2	8.0	0.0	1.0	3.0	0.25
3	0.0	−4.0	2.0	3.0	0.30
4	−3.0	3.0	1.0	3.0	0.25

One feature chosen for this example is the fact that the second and the fourth scattering structures have the same shape. This permits a numerical saving because $R_m^2(r_2) = R_m^4(r_4)$ for $1 < r_2/h_0 = r_4/h_0 < 3$, so the number of times we must approximate a solution to an initial-value problem is reduced. (This is not to say that $\eta(x, y)$ will be the same near (x_2, y_2) and (x_4, y_4), of course, since we can expect that $A_m^2 \neq A_m^4$ and $B_m^2 \neq B_m^4$, in general.) This property of the current solution procedure will be significant, if the problem in hand involves many repetitions of the same scatterer; numerical solutions to a differential equation need only be found once per scatterer, for each value of m.

Figure 3 shows the free-surface elevation in the case where $Kh_0 = 1$ and $\beta = \pi/3$. The dotted circles show the radii a_j/h_0 and b_j/h_0 centred at $(x_j/h_0, y_j/h_0)$ for $j = 1, \ldots, 4$. Numerical solutions in the four annular regions where h varies were found using (2.3). If (2.4) is used instead, then we obtain contours which, to the eye, are almost identical to those shown in Fig. 3. Another comparison we can
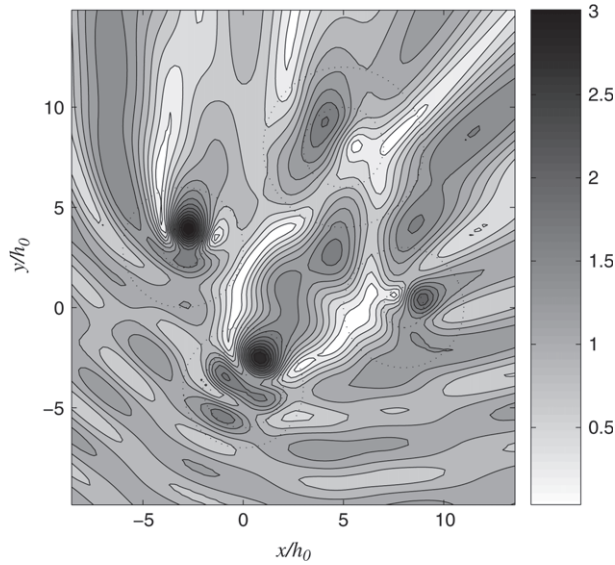

FIG. 3. Absolute free-surface elevation $|\eta(x, y)|$ computed using (2.3). This case corresponds to an incident angle $\beta = \frac{\pi}{3}$.
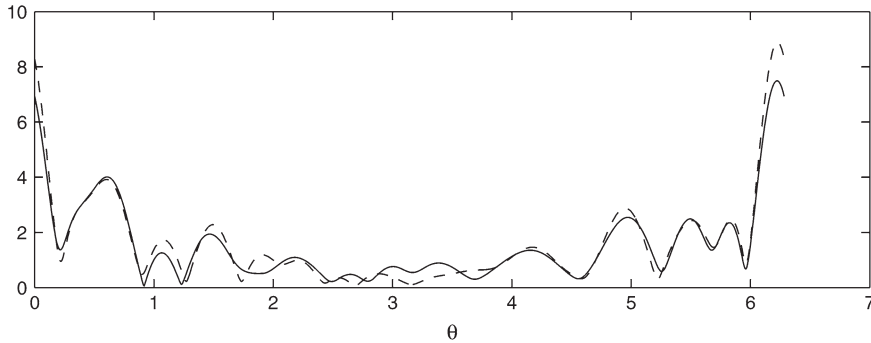

FIG. 4. Far-field coefficient $|\mathcal{F}(0, \theta)|$ corresponding to an incident angle $\beta = 0$ for the submerged topography test problem. The solid line was computed using (2.3) and the broken line using (2.4).
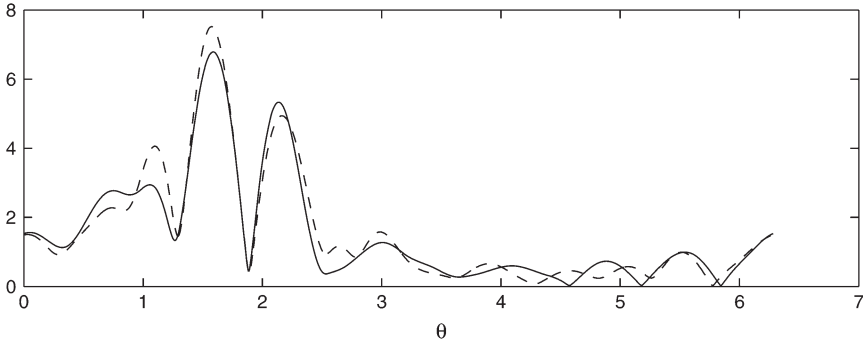
FIG. 5. Far-field coefficient $|\mathcal{F}(\frac{\pi}{2}, \theta)|$ corresponding to an incident angle $\beta = \frac{\pi}{2}$ for the submerged topography test problem. The solid line was computed using (2.3) and the broken line using (2.4).

make concerns the far-field coefficient $\mathcal{F}(\beta, \theta)$. Figure 4 considers the case $\beta = 0$ and we see that the two models (2.3) and (2.4) are in very good agreement, both predicting similar behaviour in respect of the position and magnitude of the peaks in $\mathcal{F}$.

Corresponding comparisons have been made for β taking many values between 0 and 2π and the behaviour seen in Fig. 4 for $\beta = 0$ is typical. For example, the case $\beta = \frac{\pi}{2}$ is shown in Fig. 5.

6.2 *Maniar and Newman test problem*

Maniar & Newman (1997) considered wave diffraction by a linear array of bottom-seated cylinders and found that the forces acting on (e.g.) the middle cylinder can be greatly increased, compared to the forces acting on an isolated cylinder. Here, we will consider one of their test problems.

To replicate already published results, we let $N = 9$, $x_j/h_0 = -20 + 4j$, $y_j = 0$, $a_j/h_0 = b_j/h_0 = 1$, for $j = 1, 2, \cdots, 9$, and take each structure to be of the type shown in Fig. 2(c). (This is the '$\frac{a}{d} = \frac{1}{2}$' case, in Maniar and Newman's notation.) The horizontal wave load in response to head waves ($\beta = 0$), normalized with respect to unit cylinder radius, h_0, ρ and g is shown plotted against $2K/\pi$ (equal to Kd/π in Maniar and Newman's notation) as a solid line in Fig. 6(a) and 6(b), the second figure concentrating attention near the principal peak in force. The broken line in Fig. 6(a) shows the force acting on an isolated cylinder and was included by Maniar and Newman to show the significant magnification caused by the addition of the other eight cylinders.

We now investigate how the force is affected, if we introduce a shoal around just one of the cylinders. To this end, we redefine $b_3/h_0 = 2.5$ with a view to the third cylinder, centred at $(x_3, y_3) = (-8h_0, 0)$, now being of the type considered in Fig. 2(b). The shape of the shoal is taken to be one of the simple profiles considered in the previous test problem:

$$h(r_3) = \frac{1}{2}(h_0 + h_3 - (h_3 - h_0)\cos(\pi(b_3 - r_3)/(b_3 - a_3))), \quad a_3 \leqslant r_3 \leqslant b_3.$$

Figure 6(b) shows the (normalized) force near its largest local maximum. The dotted line is for the case $h_3 = 0.05h_0$, the 'dash–dot' line is for $h_3 = 0.15h_0$ and the evenly broken line is for $h_3 = 0.25h_0$. The solid line once again gives the Maniar and Newman curve, which we may think of as corresponding to $h_3 = h_0$. We see that the peak in force on the fifth cylinder is decreased by the inclusion of a shoal on the third cylinder and that the decrease is more apparent for a larger departure from constant depth.
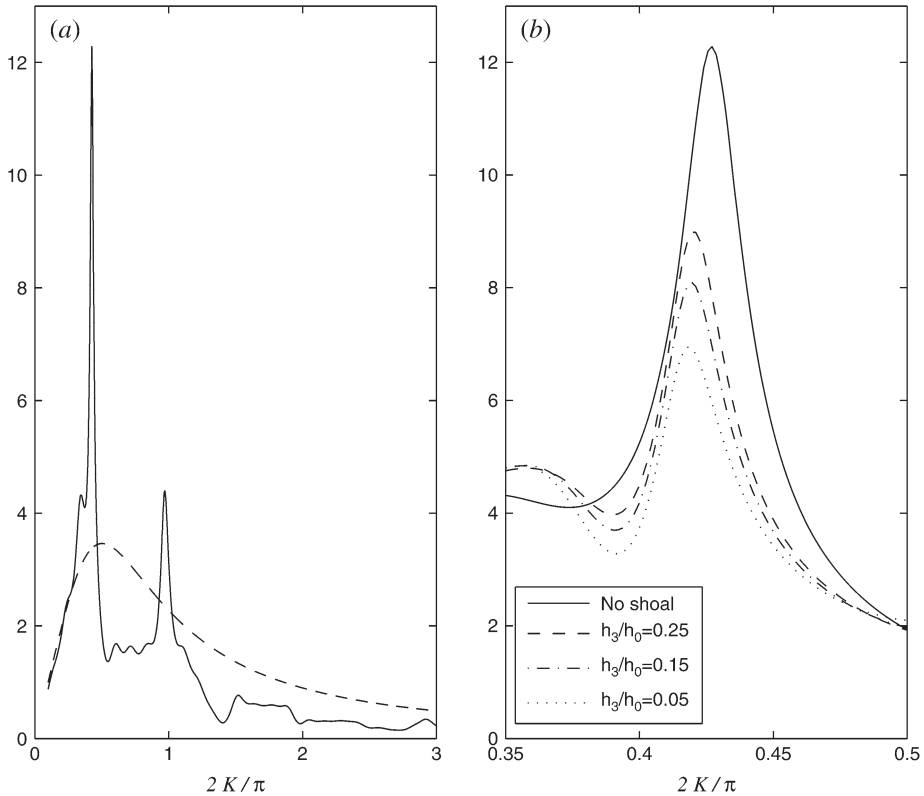
FIG. 6. Normalized force acting on a vertical cylinder in the Maniar and Newman test problem. In Fig. 6(a), the solid line shows the force acting on the fifth of nine cylinders and the broken line shows the corresponding force on an isolated cylinder (these curves were given in Fig. 1b of Maniar and Newman). In Fig. 6(b), the solid line is the same as in Fig. 6(a) and the broken lines show the change in the force acting on the fifth cylinder when the third cylinder has a shoal, as described in the text, put around it.

The local maximum in force is 12.281 (to three decimal places) when $h_3/h_0 = 1$ and this is reduced, e.g. to 6.946 (to three decimal places computed using (2.3)) when $h_3/h_0 = 0.05$. Those two data points form part of the curve shown in Fig. 7, which shows the normalized force plotted against h_3/h_0. Values of $h_3/h_0 > 1$ correspond to a trench dug around the base of the third cylinder and are included for completeness. Figure 7 also serves to show how the two mild-slope models (2.3) and (2.4) compare for this test problem, with results from the simplified model being given by a broken line: clearly, the agreement is very good.

To make it clear that the effect of the shoal (or trench) is not just on the fifth cylinder, we now give some free-surface elevation plots. Figure 8 shows the free-surface elevation $|\eta(x, y)|$ computed using (2.3) for four different values of h_3/h_0. The topmost plot corresponds to $h_3/h_0 = 1.5$, the second plot to $h_3/h_0 = 1$ (so that this plot shows $|\eta|$ for the Maniar and Newman test problem involving constant depth) and the third and the fourth plots show results corresponding to $h_3/h_0 = 0.5$ and 0.05, respectively.

In the first plot, we see that the inclusion of a trench with $h_3/h_0 = 1.5$ around the third cylinder causes an increase in wave height to the left, when compared with the contours for the Maniar and
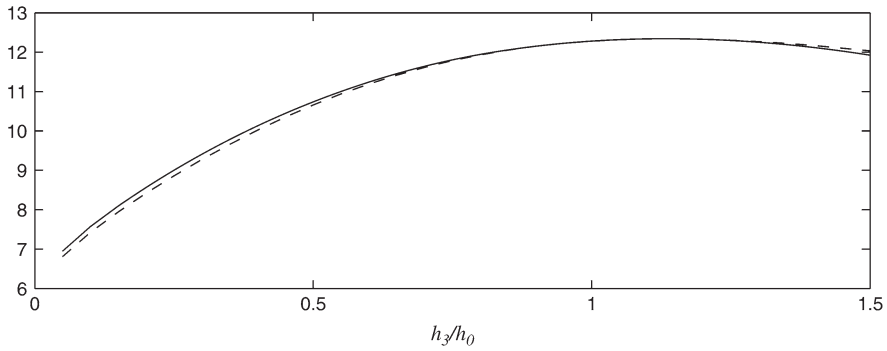
FIG. 7. Maximum normalized force on the fifth cylinder plotted against h_3/h_0. Values of $h_3/h_0 < 1$ correspond to a shoal built around the third cylinder, values of $h_3/h_0 > 1$ correspond to a trench dug around that cylinder. The solid line was computed using (2.3) and the broken line with (2.4).
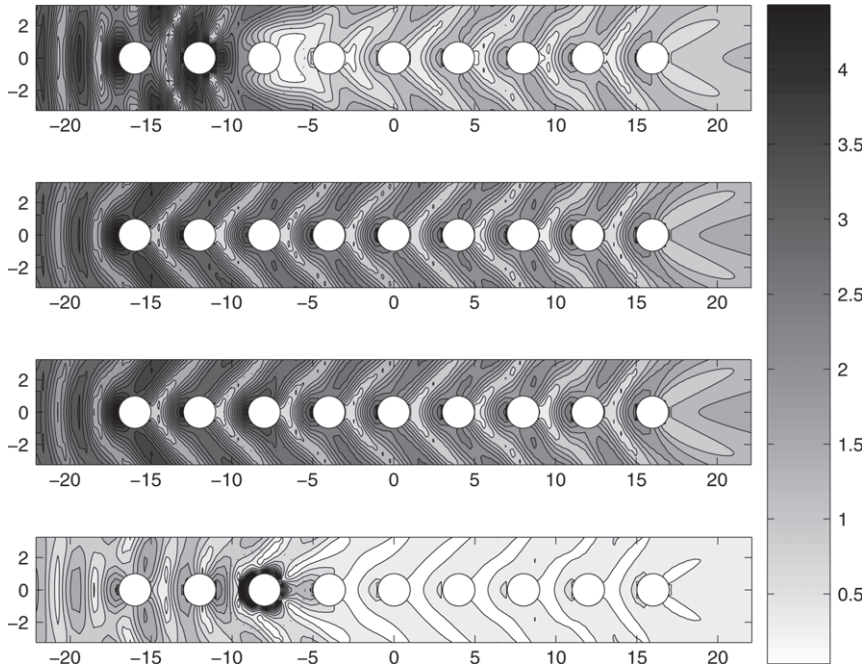

FIG. 8. Free-surface elevation $|\eta(x, y)|$ for variations on the Maniar and Newman test problem. From top to bottom, we have $h_3/h_0 = 1.50,\ 1.00,\ 0.50$ and 0.05, respectively.

Newman case of $h_3/h_0 = 1$, but that $|\eta|$ is reduced to the right. The third plot shows that the inclusion of a shoal occupying up to one-half the quiescent depth has little effect. In the fourth plot, $h_3/h_0 = 0.05$ and the effect here is that the free-surface elevation is increased near the modified cylinder, but that there is a significant reduction in wave height in the vicinity of the other eight cylinders.

7. Conclusions

Interaction theory has been adapted for use in a range of problems involving regions of varying quiescent depth. This ultimately reduces the problem to a simple numerical calculation involving some initial-value problems and a linear system. The method was applied first to a test problem involving a finite array of submerged circular islands.

There may be some interest in coastal engineering applications where topographic features can reduce wave loading and free-surface elevation. Some numerical evidence has been given to show how both these quantities can be reduced in a test problem previously considered by Maniar and Newman.

There remains, as an open question, how to solve an 'inverse problem' in which we state in advance what maximum in (say) free-surface elevation can be tolerated and then seek to find adjustments to a given array of columns or to the nearby quiescent depth to achieve that goal. We have made no attempt at this inverse problem, except of course that one must be able to solve the forward problem first and the approach described here is an efficient method for the scattering problem.

As something of an aside, we have also looked into the revised mild-slope equation (2.4) of Porter (2003). We have found that agreement with the modified mild-slope equation is excellent. Further extensive numerical experimentation has been carried out and there is strong evidence that (2.4) should now be considered as 'state of the art' in its class, for it combines simplicity (e.g. no derivatives of h are required) with accuracy.

REFERENCES

BERKHOFF, J. C. W. (1973) Computation of combined refraction-diffraction. *Proceedings 13th International Conference on Coastal Engineering, July 1972, Vancouver, Canada*, vol. 2. ASCE, pp. 471–490.

BERKHOFF, J. C. W. (1976) Mathematical models for simple harmonic linear waves. Wave diffraction and refraction. *Ph. D. Thesis*, Technical University of Delft.

CHAMBERLAIN, P. G. (2004) The effect of evanescent wave modes on scattering and near-trapping. *IMA J. Appl. Math.*, **69**, 205–218.

CHAMBERLAIN, P. G. & PORTER, D. (1995) The modified mild-slope equation. *J. Fluid Mech.*, **291**, 393–407.

CHAMBERLAIN, P. G. & PORTER, D. (1999) Scattering and near-trapping of water waves by axisymmetric topography. *J. Fluid Mech.*, **388**, 335–354.

GRADSHTEYN, I. S. & RYZHIK, I. M. (1965) *Tables of Integrals, Series and Products*. New York: Academic Press.

HOMMA, S. (1950) On the behaviour of seismic sea waves around a circular island. *Geophys. Mag.*, **XXI**, 199–208.

HUGHES, C. M. (2005) On the topographical scattering and near-trapping of water waves. *Ph.D. Thesis*, The University of Reading. Reading.

KIRBY, J. T. (1986) A general wave equation for waves over rippled beds. *J. Fluid Mech.*, **162**, 171–186.

LINTON, C. M. & EVANS, D. V. (1990) The interaction of waves with arrays of vertical circular cylinders. *J. Fluid Mech.*, **215**, 549–569.

MANIAR, H. D. & NEWMAN, J. N. (1997) Wave diffraction by a long array of cylinders. *J. Fluid Mech.*, **339**, 309–329.

PORTER, D. (2003) The mild slope equations. *J. Fluid Mech.*, **494**, 51–63.

PORTER, D. & STAZIKER, D. J. (1995) Extensions of the mild slope equation. *J. Fluid Mech.*, **300**, 367–382.

SILVA, R., BORTHWICK, A. G. L. & EATOCK TAYLOR, R. (2005) Numerical implementation of the harmonic modified mild-slope equation. *Coast. Eng.*, **52**, 391–407.

SMITH, R. & SPRINKS, T. (1975) Scattering of surface waves by a conical island. *J. Fluid Mech.*, **72**, 373–384.

SPRING, B. H. & MONKMEYER, P. L. (1974) Interaction of plane waves with vertical cylinders. *Proceedings 14th International Coastal Engineering*, copenhagen chapter 107, pp. 1828–1845.

WALKER, D. A. G. & EATOCK TAYLOR, R. (2005) Wave diffraction from linear arrays of cylinders. *Ocean Eng.*, **32**, 2053–2078.